Journal of Alloys and Compounds 488 (2009) 117–122

Contents lists available at ScienceDirect

Journal of Alloys and Compounds

journal homepage: www.elsevier.com/locate/jallcom

Effect of fabrication methods on microstructure and mechanical properties of Fe_3Al-based alloys

Jian Wang[a,*], Jiandong Xing[a], Zhibin Qiu[a], Xiaohui Zhi[b], Li Cao[a]

[a] State Key Laboratory for Mechanical Behavior of Materials, Xi'an Jiaotong University, Xi'an 710049, Shaanxi Province, PR China
[b] School of Mechanical Engineering, Shijiazhuang Railway Institute, Shijiazhuang 050043, Hebei Province, PR China

ARTICLE INFO

Article history:
Received 20 July 2009
Received in revised form 27 August 2009
Accepted 28 August 2009
Available online 2 September 2009

Keywords:
Fe_3Al
Plasma activated sintering
Hot pressing
Hardness
Toughness

ABSTRACT

Disordered Fe(Al) solid solution powders with nano-grain size were fabricated by mechanical alloying, and subsequently the milled powders were consolidated by plasma activated sintering (PAS) and hot pressing (HP), respectively. The effect of the two fabrication methods on microstructure and mechanical properties of Fe_3Al was investigated. Disordered Fe_3Al with submicron-grain size was obtained by PAS, while ordered Fe_3Al with micron-grain size was obtained by HP. Compared with ordered Fe_3Al with micron-grain size by HP, disordered Fe_3Al with submicron-grain size by PAS had higher hardness and toughness. $Fe_3AlC_{0.5}$ was precipitated in all specimens with methanol addition during mechanic alloying. The precipitation of $Fe_3AlC_{0.5}$ improved the hardness of Fe_3Al, but was harmful to the toughness of Fe_3Al.

1. Introduction

Fe_3Al-based intermetallics (Fe_3Al) have attracted considerable attention as potential candidates for high temperature structural materials, because of their good oxidation resistance and excellent sulfidation resistance. However, likewise in the other intermetallics, the main drawback concerning their possible technological applications is their low ductility in the cast form at room temperature and processing problems [1–5].

Some authors have attempted to improve the ductility of Fe_3Al using powder metallurgy (PM) processing, which could obtain Fe_3Al with relatively fine grains [6–14]. However, slight improvements in ductility have been achieved by using conventional PM processing such as pressure less sintering and hot pressing (HP) [14]. Recently, considerable attention has been given to the development of nanocrystalline intermetallics [15]. Some authors have used nanocrystalline prealloyed powders, which can be easily produced by mechanical alloying (MA) [16–22], as starting materials to fabricate nanocrystalline intermetallics. However, the full benefit of such nanocrystalline powders may be preserved only if the consolidation process can eliminate extensive growth. Plasma activated sintering (PAS), also known as spark plasma sintering (SPS), is a consolidation method which has the capability of retaining the fine grain size of the starting powders while producing near theoretical density materials [23–26]. In the present study, nanocrystalline prealloyed powders were fabricated by MA, and two different consolidation methods, PAS and HP, were used to fabricate Fe_3Al. The effect of the two fabrication methods on the microstructure and mechanical properties of Fe_3Al was studied.

2. Experimental procedure

The MA was performed in a planetary ball mill at 250 rpm for 50 h under an argon atmosphere. Iron powder and aluminum powder were mixed in composition of Fe–28 at.% Al. The iron powder and aluminum powder used were all in the size of 200 mesh and in the purity of 99 wt.%. Stainless steel balls and vial were used, and the ball-to-powder ratio was 10:1. Certain amount of methanol is added to the powder mixture during milling to reduce the effect of cold welding. Four batches of as-milled powders, with the methanol addition amount of 0, 0.5, 1.0, 1.5 ml respectively, were obtained, and they were named as A, B, C, and D in sequence.

Graphite mould was used during the PAS process, the inner surface was covered with thin carbolic papers. The apparatus is the Ed-PAS III sintering system produced by Elenix Ltd. with a vacuum of 2 Pa in its chamber. The milled powders were compacted into the graphite mould under a continuous pressure of 30 MPa. The powders were heated up at the rate of 2 K/s, and then consolidated at 1273 K for 180 s. The cooling rate was about 1 K/s after consolidation. The whole time used was about 30 min.

During the HP process, the milled powders were also compacted in a graphite mould under a continuous pressure of 30 MPa using a HP apparatus with a vacuum of 1.33×10^{-2} Pa in its chamber. The milled powders were heated up at the rate of 13 K/min, and consolidated at 1473 K for 30 min followed by furnace cooling. The whole time used was about 10 h.

The specimens and their treatments are shown in Table 1.

Phase analyses were made by XRD and densities were measured by the Archimede's method. The phase constitution and microstructure of the specimens

* Corresponding author at: School of Materials Science and Engineering, Xi'an Jiaotong University, 28 Xianning West Road, Xi'an 710049, Shaanxi Province, PR China. Tel.: +86 29 82665636; fax: +86 29 82665479.
E-mail address: jwangxjtu@163.com (J. Wang).

0925-8388/$ – see front matter © 2009 Elsevier B.V. All rights reserved.
doi:10.1016/j.jallcom.2009.08.138

Table 1
The specimens and their treatments.

Specimens	Methanol addition amounts (ml) during MA	Consolidation method
PAS-A	0	PAS
PAS-B	0.5	
PAS-C	1.0	
PAS-D	1.5	
HP-A	0	HP
HP-B	0.5	
HP-C	1.0	
HP-D	1.5	

were characterized using scanning electron microscope (SEM) equipped with an energy dispersive X-ray analyzer (EDS) and transmission electron microscope (TEM).

The bulk hardness (HRC) of the specimens was determined by the mean of five measurements using HRS-150 Digital Rockwell Hardness Machine. Rectangular bars for the fracture toughness tests were cut using an electro-discharge machine from the sintered samples. Single edge notched bend (SENB) specimens, with a precrack of a/W ratio about 0.5, were ground and polished to the final dimensions of 3 mm × 5 mm × 20 mm. The fracture toughness measurements were carried out using a three-point bending test (INSTRON-1195) with a cross-head speed of 0.5 mm/min. At least three bars were measured for each material. The fracture toughness K_{IC} was calculated using Eqs. (1) and (2) [27].

$$K_{IC} = Y\frac{3PL}{2bW^2}\cdot a^{1/2} \quad (1)$$

$$Y = 1.93 - 3.07\frac{a}{W} + 14.53\left(\frac{a}{W}\right)^2 - 25.11\left(\frac{a}{W}\right)^3 + 25.80\left(\frac{a}{W}\right)^4 \quad (2)$$

where Y is the geometrical factor related to the crack depth ratio, P is the maximum load, b is the width of the bar, L is the length of the bar, W is the thickness of the bar, and a is the initial crack length.

3. Results

3.1. XRD patterns of the as-milled powders

XRD patterns of the as-milled powders are presented in Fig. 1. No superlattice reflection peaks are found in the milled powders, and thus it can be deduced that disordered Fe(Al) solid solution formed after milling. Peak broadening is also observed in Fig. 1, which may be caused by grain size refinement or internal stresses [28]. Warren–Averbach method [29] was used to estimate the grain size of the as-milled powders, and the results indicated that their mean grain size is in the range of 9–16 nm.

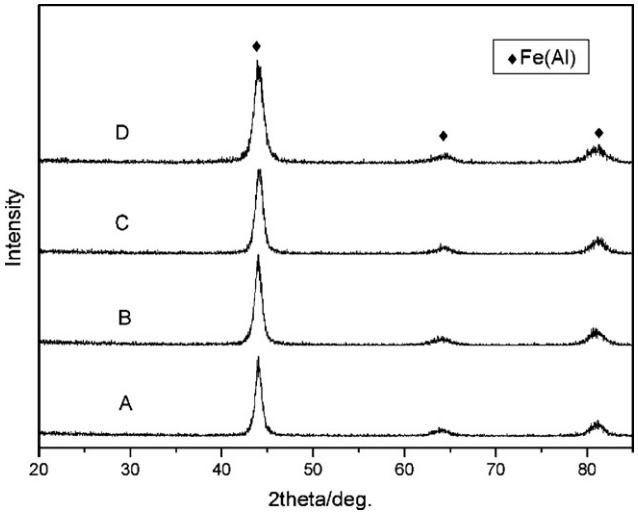

Fig. 1. XRD patterns of milled powders.

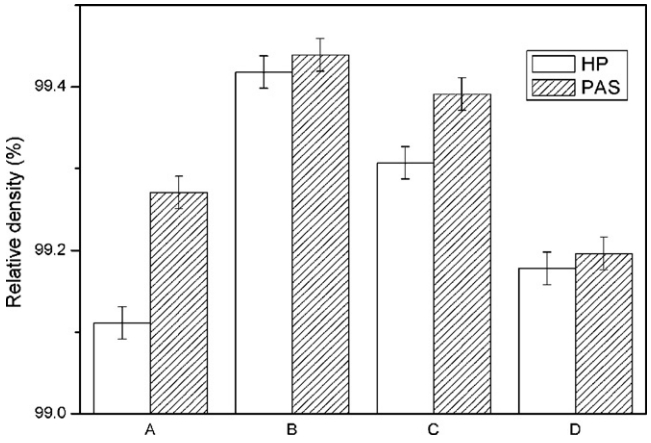

Fig. 2. Relative densities of Fe_3Al alloys consolidated by PAS and HP.

3.2. Microstructure of the as-consolidated Fe_3Al

Fig. 2 shows the relatively density of Fe_3Al consolidated by two methods. From Fig. 2, it can be seen that the relative density of each specimen is more than 99%, and the optimum is for 0.5 ml-sample B. XRD patterns of Fe_3Al consolidated by PAS and HP are present in Fig. 3(a) and (b), respectively. From Fig. 3, it can be seen that the peaks of $Fe_3AlC_{0.5}$ are apparently observed in all specimens with methanol addition during MA. This indicates that $Fe_3AlC_{0.5}$ was precipitated in those specimens, and that the precipitation of $Fe_3AlC_{0.5}$ is due to the methanol addition during MA. It is noted the peaks of $Fe_3AlC_{0.5}$ are observed in HP-A specimen without methanol addition during MA because of the diffusion of C from the graphite mould during sintering and holding process. Superlattice reflection peaks are not found in specimens by PAS, and it indicates that disordered Fe(Al) solid solution, which was formed after milling, was retained in specimens by PAS. In addition, it can be seen that the maximum of Fe(Al) line moves depending on methanol content. The lattice parameters for Fe(Al) of four series specimens by PAS are 0.28851, 0.28845, 0.28838 and 0.28844 nm, respectively. These parameters suggest that the precipitation of $Fe_3AlC_{0.5}$ from the supersaturated solid solution of Fe(Al) phase low the concentration of aluminum and carbon in matrix phase, resulting in the decrease of lattice parameter. In contrast with specimens by PAS, superlattice reflection peaks are observed in specimens by HP, and it indicates that disordered Fe(Al) solid solution transferred to ordered Fe_3Al after HP. The long-range parameter S can be evaluated by measuring the intensity of the superlattice reflections relative to that of the fundamental reflections according to Eq. (3) [29]:

$$S = \sqrt{\frac{I_S(\text{dis})/I_F(\text{dis})}{I_S(\text{ord})/I_F(\text{ord})}} \quad (3)$$

where I_S and I_F represent the integrated intensities of the superlattice and fundamental reflection, respectively, and the subscripts (dis) and (ord) refer to the disordered and ordered states, respectively. The tested results are summarized in Table 2. It can be seen

Table 2
Long-range parameter S of specimens consolidated by HP.

Specimens	I_S (111)	I_F (220)	S
Completely ordered[a]	74	999	1
HP-A	428	10,687	0.74
HP-B	321	8,996	0.69
HP-C	178	6,666	0.60
HP-D	103	7,977	0.42

[a] According to PDF 65-3006.

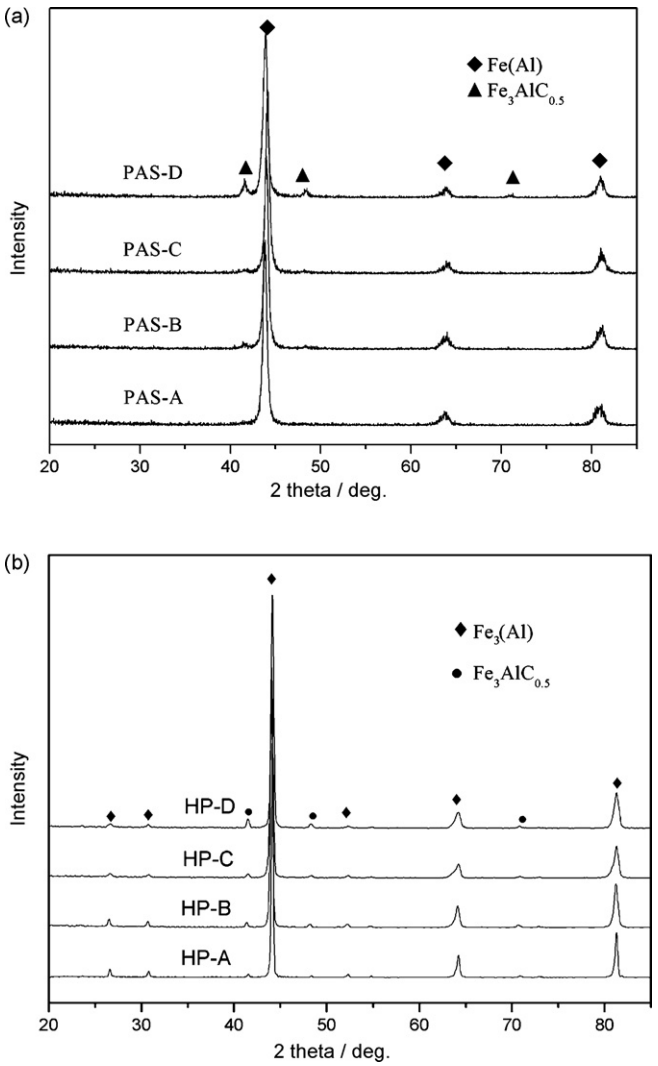

Fig. 3. X-ray diffraction profiles of Fe_3Al consolidated by PAS (a) and HP (b).

that, with increase of methanol addition during MA, the long-range parameter *S* decreases.

Fig. 4 shows the typical SEM images of specimens by PAS or HP (etched with ethanol–20 wt.% nitric acid). Two areas with different colors (dark and gray) are observed in all specimens. In addition, precipitates, $Fe_3AlC_{0.5}$, are also observed in specimens with methanol addition during MA (Fig. 4(b) and (d)). It also can be seen that the size of the precipitates in specimen by PAS is smaller than that in specimen by HP. EDS results of the points marked in Fig. 4(a) and (c) are summarized in Table 3. From Table 3, it can be seen that the concentration of Al in gray areas is higher than that in dark areas. According to the X-ray diffraction results in Fig. 3, it can be deduced that the two areas with different colors in Fig. 4 are the same phase constitution. Fig. 5 shows the TEM microstructure and the selected area electron diffraction patterns (SADP) of PAS-A and HP-A. It can be seen that the grain size of disordered Fe_3Al by PAS and ordered Fe_3Al by HP are about 300 nm and 1 μm respectively, which are far more smaller than that of as-casting Fe_3Al [30]. From Fig. 5, it can also be deduced that the reordering and significant grain growth occurred during HP and ordering did not occur during PAS. Compared with the size of the milled powders (9–16 nm), grain size of specimen by PAS became bigger despite its relatively high cooling rate, but it is far smaller than that of specimen by HP.

Table 3
EDS results of the points marked in Fig. 4.

Position	Fe (at.%)	Al (at.%)	Cr (at.%)
1	69.90	27.80	2.30
2	75.17	22.78	2.05
3	70.68	27.08	2.24
4	73.61	24.07	2.32

3.3. Hardness and fracture toughness of the specimens

Figs. 6 and 7 show the hardness (HRC) and fracture toughness (K_{IC}) of Fe_3Al consolidated by two methods, respectively. Hardness [31] and fracture toughness [32] of as-casting Fe_3Al also present in Figs. 6 and 7. It can be seen that the hardness of Fe_3Al by PAS or HP is much higher than that of as-casting Fe_3Al, but that the toughness of Fe_3Al by HP is lower than that of as-casting Fe_3Al. In addition, with the increase of methanol addition during MA, the hardness of all specimens increased, but the toughness of all specimens decreased. Fig. 8 shows the typical fracture surface of the specimens. Transgranular fracture, which was the normal fracture mode in as-casting pure Fe_3Al [30,33], is significant in the specimens by HP, while the specimens by PAS shows partly plastically deformed zones.

4. Discussion

4.1. Reordering during consolidation

The as-milled powders consist of only disordered Fe(Al) solid solution, which is metastable according to the phase diagram of Fe–Al [34]. The reordering during consolidation is driven by the ordering energy (the energy difference between ordered and disordered states). The ordering energy (−9 kJ/mol) can be estimated from the formation enthalpies of Fe_3Al (−18 kJ/mol [9]) according to the Bragg–Williams theory [35] ($\Delta H_{ord} = 0.5\Delta H_f$). It can be seen that ordering energy of Fe_3Al is significantly lower, so its tendency to reordering is lower. In general, the time required for the reordering of as-casting Fe_3Al is about few days [30]. In the present study, the cooling rate is relatively high during PAS, so the reordering could not occur and the disordered phase was retained. In contrast, the cooling rate during HP is relatively low and partly ordered Fe_3Al were obtained. The increase of reordering rate of specimen by HP is due to the large grain boundary energy and elastic energy stored in the milled nanocrystalline powders. Tang [21] also obtained ordered Fe_3Al by annealing the milled disordered powder at 1073–1373 K.

4.2. Precipitation of $Fe_3AlC_{0.5}$ and the loss of Al

From Fig. 3, it can be seen that the peaks of $Fe_3AlC_{0.5}$ are apparently observed in all specimens with methanol addition during MA. This indicates that $Fe_3AlC_{0.5}$ was precipitated in those specimens, and that the precipitation of $Fe_3AlC_{0.5}$ is due to the methanol addition during MA. The higher the sintering temperature and lower the cooling rate, the bigger the precipitated $Fe_3AlC_{0.5}$ carbides. The sintering temperature (1473 K) of HP is higher than that of PAS (1273 K), and the cooling rate of HP is far lower than that of PAS, so the $Fe_3AlC_{0.5}$ carbides in specimens by HP are bigger than that in specimens by PAS (Fig. 4(b) and (d)). Palm and Inden [36] has also found that the solubility of carbon within the Fe(Al) solid solution was up to 1.5 at.% and precipitation of the $Fe_3AlC_{0.5}$ formed at the temperature beneath 973 K.

Two areas with different colors, which has the same phase constitute, were observed in the all specimens. The same phenomena were also observed Ni_3Al [37] consolidated from the milled solid solution powders. The EDS results show the Al concentration in the

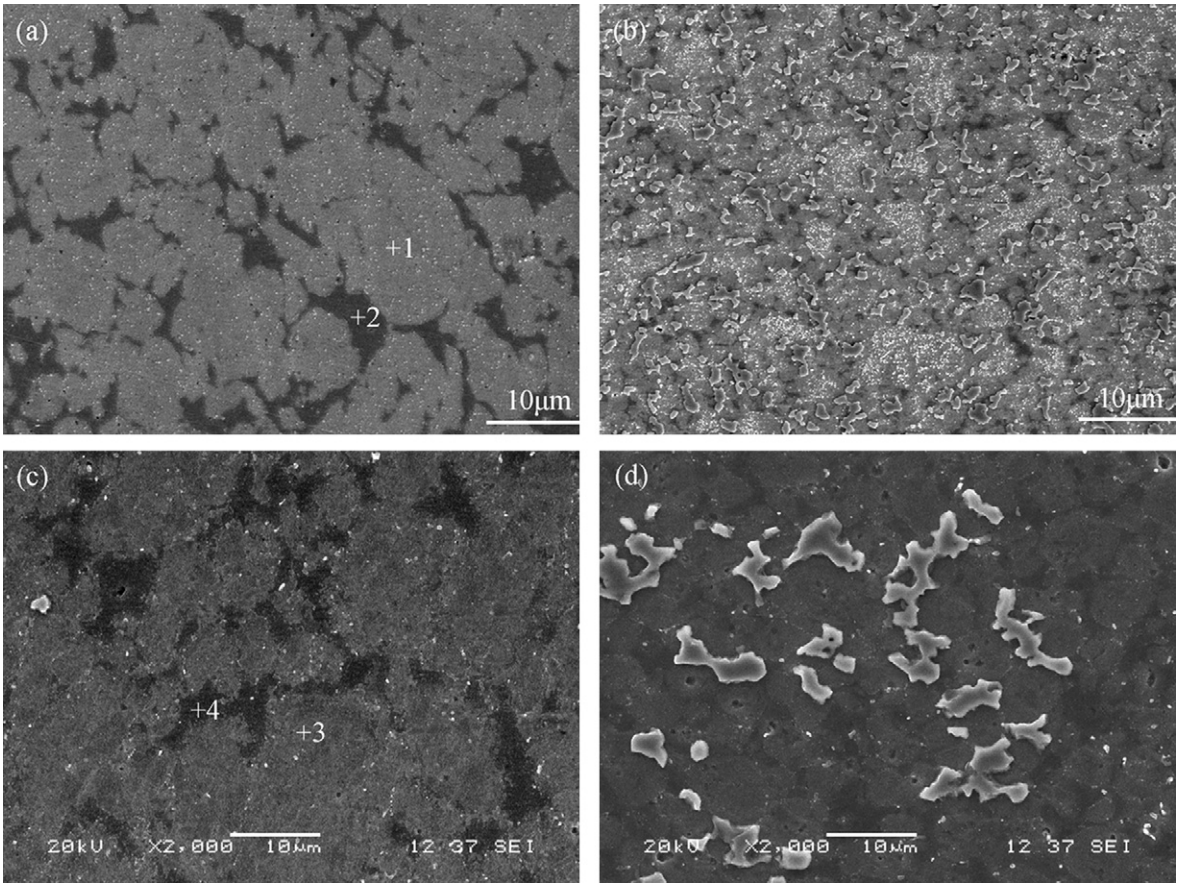

Fig. 4. SEM images of consolidated specimens (etched with ethanol–20 wt.% nitric acid) (a) PAS-A, (b) PAS-D, (c) HP-A, and (d) HP-D.

dark areas is slightly lower than that in the gray areas. The loss of Al could be explained by the volatilization of Al in vacuum and at high temperature during consolidation. The effect of vacuum level on the steam point of Al and Fe is summarized in Table 4. During HP, the working pressure is 1.33×10^{-2} Pa, and the consolidation temperature is higher than the steam point of Al, so Al in the surface of the milled powders firstly volatilized during consolidation and the dark area around the gray area formed after consolidation. Although the sintering temperature did not reached to the steam point of Al during PAS, the heat effect created by plasma may also cause the volatilization of Al in the surface of the milled powder. The loss of Al could decrease the corrosion resistance, and so two areas with different colors were observed in the etched specimens.

4.3. Effect of microstructure on mechanical properties of Fe_3Al

It is well known that hardness of materials can be improved by refining grain size and precipitation of hard phases. In the present study, the grain size of as-consolidated Fe_3Al is much smaller than that of as-casting Fe_3Al [30], and so the hardness of the as-consolidated Fe_3Al was improved. In addition, hard $Fe_3AlC_{0.5}$ was precipitated in the specimen with methanol addition during MA, so the hardness increased with increasing the methanol.

In specimens by PAS, Fe_3Al is disordered and its strengthening mechanisms are mainly fine grain strengthening and precipitation strengthening. In specimens by HP, Fe_3Al is ordered Fe_3Al and its strengthening mechanisms are fine grain strengthening, precipitation strengthening, and ordering strengthening. This ordering in specimens by HP can be disrupted by the passing dislocation, forming a so-called anti-phase boundary (APB), and an additional surface energy has to be provided by the external work and thus raises the hardness or strength of the specimens [39]. Therefore, although the grain size of specimens by PAS is far smaller than that of specimens by HP, the hardness of specimens by PAS is only slightly higher than that of specimens by HP although the grain size of specimens by PAS is obviously smaller than that of specimens by HP (Fig. 6).

Grain size and ordering degree have obviously effect on the toughness of intermetallics. For disordered Fe_3Al by PAS, like conventional materials, their toughness can be improved by grain refinement, so disordered Fe_3Al with submicron-grain size has relatively higher fracture toughness. For ordered Fe_3Al, the dislocation motion can be blocked by the APB, so the toughness of ordered Fe_3Al fabricated by HP is lower than that of the as-casting Fe_3Al, although the grain size of Fe_3Al fabricated by HP is smaller than that of the as-casting Fe_3Al [30]. In addition, the amount and size of

Table 4
Effect of vacuum level on the steam point of Al and Fe [38].

Element	Steam point (K)				
	1.33×10^{-3} Pa	1.33×10^{-2} Pa	1.33×10^{-1} Pa	1.33 Pa	1.33×10^{-1} Pa
Al	1114	1200	1301	1421	1566
Fe	1356	1453	1566	1698	1859

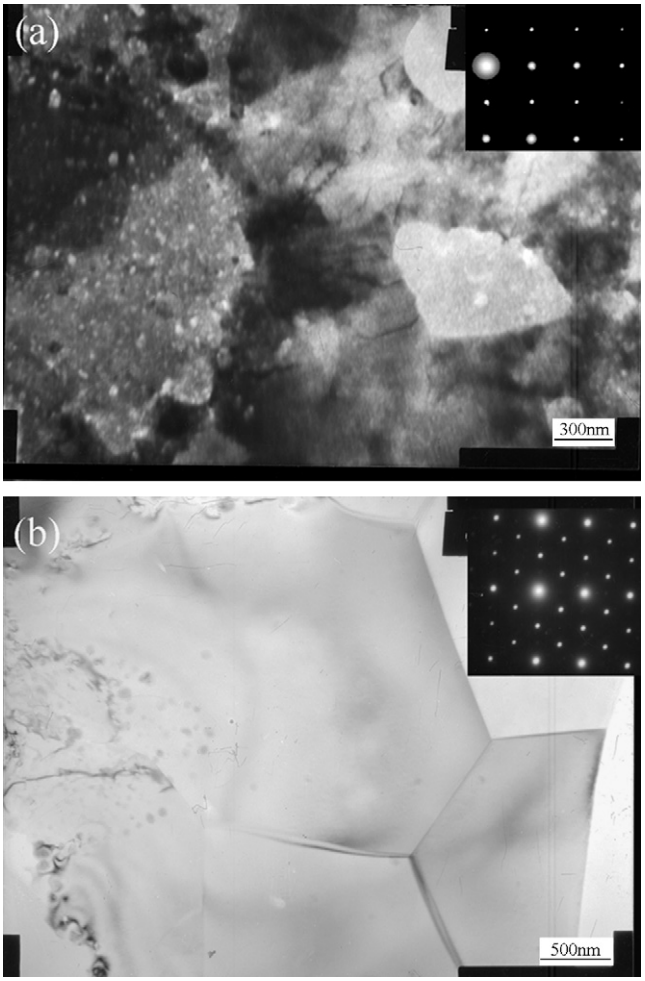

Fig. 5. Transmission electron micrographs and selected area electron diffraction patterns of the consolidated specimens (a) PAS-A and (b) HP-A.

precipitates has obviously effect on the toughness of materials. The toughness of materials decreases with increase of the precipitated amounts and size [40], so the toughness of specimens decreased with increase of methanol. Compared with specimens by PAS with the same addition of methanol during MA, specimens by HP have large precipitates, so their toughness is lower.

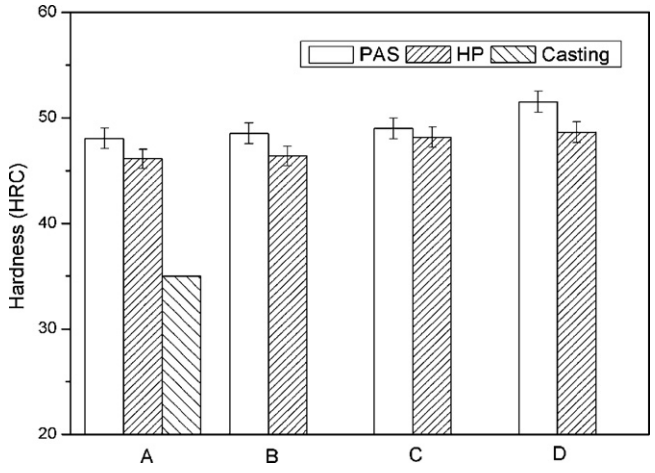

Fig. 6. Hardness of Fe_3Al alloys fabricated by different process.

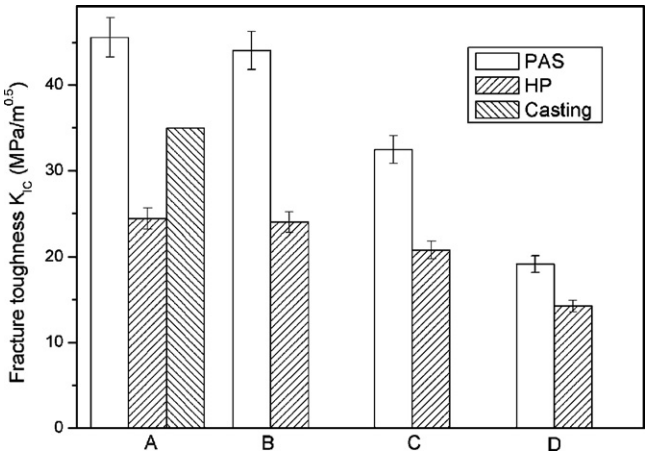

Fig. 7. Fracture toughness of Fe_3Al alloys fabricated by different process.

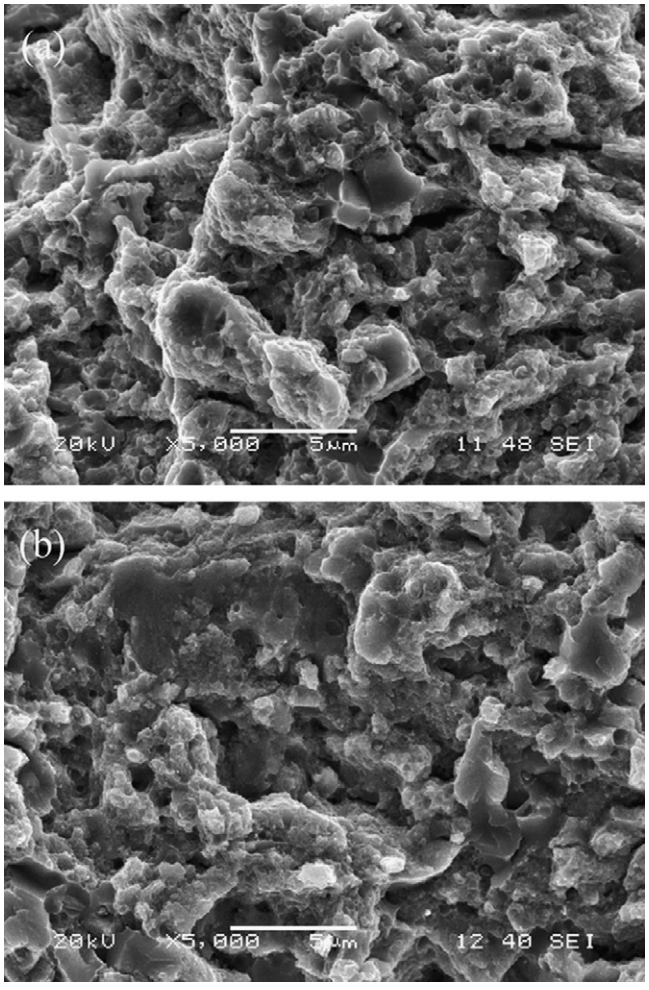

Fig. 8. Fracture surfaces of (a) PAS-A and (b) HP-A.

5. Conclusions

(1) Disordered and ordered Fe_3Al were fabricated by PAS and HP from milled nanocrystalline Fe(Al) solid solution powders, respectively.
(2) Compared with ordered Fe_3Al with micron-grain size by HP, disordered Fe_3Al with submicron-grain size by PAS had higher hardness and toughness. The strengthening mechanisms of

specimens by PAS are mainly fine grain strengthening and precipitation strengthening, while the strengthening mechanisms of specimens by HP are fine grain strengthening, precipitation strengthening, and ordering strengthening.

(3) $Fe_3AlC_{0.5}$ was precipitated in all specimens with methanol addition during mechanic alloying. The precipitation of $Fe_3AlC_{0.5}$ improved the hardness of Fe_3Al, but was harmful to the toughness of Fe_3Al.

Acknowledgement

This work was supported by the National Nature Science Foundation of China (Grant No. 50871084).

References

[1] N.S. Stoloff, Mater. Sci. Eng. A258 (1998) 1–14.
[2] C.T. Liu, J. Stringer, J.N. Mundy, et al., Intermetallics 5 (1997) 579–596.
[3] N.S. Stoloff, C.T. Liu, S.C. Deevi, Intermetallics 8 (2000) 1313–1320.
[4] S.C. Deevi, V.K. Sikka, C.T. Liu, Prog. Mater. Sci. 42 (1997) 177–192.
[5] R.S. Sunder, R.G. Baligidad, Y.K.R.K. Prasad, et al., Mater. Sci. Eng. A 258 (1998) 219–228.
[6] S. Gedevanishvili, S.C. Deevi, Mater. Sci. Eng. A 325 (2002) 163–176.
[7] D.L. Joslin, D.S. Easton, C.T. Liu, S.A. David, Mater. Sci. Eng. A 192/193 (1995) 544–548.
[8] H.-Z. Kang, C.-T. Hu, Mater. Chem. Phys. 88 (2004) 264–272.
[9] B.H. Rabin, R.N. Wright, Metall. Mater. Trans. A 22 (1991) 277–286.
[10] D.Q. Yi, C.H. Li, J.H. Wang, R. Warren, I. Olefjord, Mater. Sci. Technol. 11 (1995) 650–655.
[11] N.K. Xydas, B.L. Gabbitas, X.X. Xu, L.A. Salam, Powder Metall. 46 (2003) 68–72.
[12] N.K. Xydas, L.A. Salam, Powder Metall. 49 (2006) 146–152.
[13] H.-Z. Kang, S. Lee, C.-T. Hu, Mater. Sci. Eng. A 398 (2005) 360–366.
[14] M.G. Mendiratta, S.K. Ehlers, D.K. Chatterjee, H.A. Lipsitt, Metall. Trans. A 18 (1987) 283–291.
[15] R. Bohn, T. Haubold, R. Birringer, H. Gleiter, Scr. Metall. 25 (1991) 811–816.
[16] S.-M. Zhu, M. Tamura, K. Sakamoto, K. Iwasaki, Mater. Sci. Eng. A 292 (2000) 83–89.
[17] M. Krasnowski, T. Kulik, Intermetallics 15 (2007) 201–205.
[18] M. Krasnowski, T. Kulik, Intermetallics 15 (2007) 1377–1383.
[19] M.H. Enayati, M. Salehi, J. Mater. Sci. 40 (2005) 3933–3938.
[20] R.-H. Fan, J.-T. Sun, H.-Y. Gong, et al., Powder Technol. 149 (2005) 121–126.
[21] W.M. Tang, Z.X. Zheng, H.J. Tang, et al., Intermetallics 15 (2007) 1020–2026.
[22] G.H. Fair, J.V. Wood, Powder Metall. 36 (1993) 123–128.
[23] M. Zadra, F. Casari, I. Lonardelli, et al., Intermetallics 15 (2007) 1650–1658.
[24] M.A. Venkataswamy, J.A. Schneider, J.R. Groza, et al., Mater. Sci. Eng. A 207 (1996) 153–158.
[25] B.G. Park, S.H. Ko, Y.H. Park, et al., Intermetallics 14 (2006) 660–665.
[26] Y. Minamino, Y. Koizumi, N. Tsuji, et al., Sci. Technol. Adv. Mater. 5 (2004) 133–143.
[27] Deke Shi, Zhihao Jin, Mechanical Properties of Materials, Xi'an Jiaotong University Press, Xi'an, 1997, pp. 108–109 (in Chinese).
[28] B.D. Cullity, Elements of X-ray Diffraction, 2nd ed., Addision-Wesley, 1978.
[29] C. Suryanarayana, M.G. Norton, X-ray Diffraction: A Practical Approach, Plenum, New York, NY, 1998.
[30] C.G. Mckamey, J.A. Horton, C.T. Liu, J. Mater. Res. 4 (1989) 1156–1163.
[31] R.S. Sundar, T.R.G. Kutty, D.H. Sastry, Intermetallics 8 (2000) 427–437.
[32] S.H. Ko, R. Gnanamoorthy, S. Hanada, Mater. Sci. Eng. A 222 (1997) 133–139.
[33] R.G. Bordeau, AFWAL-TR-87-4009, Development of Iron Aluminides, Air Force Wright Aeronautical Laboratories, Wright-Patterson Air Force Base, OH, 1987.
[34] B.S. Murty, S. Ranganathan, Int. Mater. Rev. 43 (1998) 101–141.
[35] B.L. Bragg, E.J. Williams, Proc. R. Soc. A 151 (1935).
[36] M. Palm, G. Inden, Intermetallics 3 (1995) 443–454.
[37] L.D. Angelo, G. González, J. Ochoa, J. Alloys Compd. 434/435 (2007) 348–353.
[38] D. Yongnian, Y. Bin, Vacuum Metallurgy of Nonferrous Metals, Metallurgy Industry Press, Beijing, 2009 (in Chinese).
[39] J. RÖsler, H. Harders, M. Bäker, Mechanical Behaviour of Engineering Materials, Springer-Verlag, Berlin/Heidelberg, 2007.
[40] V.A. Romanova, R.R. Balokhonov, S. Schmauder, Acta Mater. 57 (2009) 97–107.